Tectonophysics 663 (2015) 110–121

Contents lists available at ScienceDirect

Tectonophysics

journal homepage: www.elsevier.com/locate/tecto

Mesozoic and Cenozoic exhumation history of the SW Iberian Variscides inferred from low-temperature thermochronology

Mercedes Vázquez-Vílchez [a,b], Antonio Jabaloy-Sánchez [c,*], Antonio Azor [c], Finlay Stuart [d], Cristina Persano [d,e], Francisco M. Alonso-Chaves [f], Luis Miguel Martín-Parra [g], Jerónimo Matas [g], Encarnación García-Navarro [f]

[a] Andean Geothermal Center of Excellence (CEGA), Universidad de Chile, Santiago, Chile
[b] Department of Geology, Universidad de Chile, Santiago, Chile
[c] Departamento de Geodinámica, Facultad de Ciencias, Universidad de Granada, Granada, Spain
[d] Isotope Geosciences Unit, Scottish Universities Environmental Research Centre, Scottish Enterprise Technology Park, East Kilbride G75 OQF, UK
[e] School of Geographical and Earth Sciences, University of Glasgow, Glasgow, UK
[f] Departamento de Geodinámica y Paleontología, Facultad de Ciencias Experimentales, Universidad de Huelva, Huelva, Spain
[g] Instituto Geológico y Minero de España, Madrid, Spain

ARTICLE INFO

Article history:
Received 31 January 2015
Received in revised form 28 May 2015
Accepted 27 June 2015
Available online 11 July 2015

Keywords:
Low-temperature thermochronometers
Exhumation history
Iberian massif
Alpine deformation
Reactivation of Variscan faults

ABSTRACT

The post-Paleozoic tectonothermal evolution of the SW Iberian Variscides is poorly known mainly due to the scarce low-temperature geochronological data available. We have obtained new apatite fission-tracks and apatite (U–Th)/He ages to constrain the Mesozoic and Cenozoic tectonic evolution of this portion of the Iberian Massif located just north of the Betic-Rif Alpine orogen.

We have obtained nine apatite fission-track ages on samples from Variscan and pre-Variscan granitoids. These ages range from 174.4 (±10.8) to 54.1 (±4.9) Ma, with mean track lengths between 10.3 and 13.9 μm. We have also performed 5 (U–Th)/He datings on some of the same samples, obtaining ages between 74.6 (±1.6) and 18.5 (±1.4) Ma. Time–temperature path modeling of these low-temperature geochronological data leads us to envisage four post-Paleozoic tectonically controlled exhumation episodes in the SW Iberian Variscides. Three of these episodes occurred in Mesozoic times (Middle Triassic to Early Jurassic, Early Cretaceous, and Late Cretaceous) at rates of ≈1.1 to 2.5 °C Ma^{-1}, separated by periods with almost no cooling. We relate these Mesozoic cooling events to the formation of important marginal reliefs during the rifting and opening of the central and northern Atlantic realm. The fourth exhumation episode occurred in Cenozoic times at rates of ≈3.2 to 3.6 °C Ma^{-1}, being only recorded in samples next to faults with topographic escarpments. These samples cooled below 80 °C at ≈20 Ma at rates of 3–13 °C Ma^{-1} due to roughly N–S oriented compressional stresses affecting the whole Iberian plate, which, in the particular case of SW Iberia, reactivated some of the previous Late Paleozoic thrusts.

1. Introduction

Orogen exhumation occurs as a combination/competition of tectonically- and gravity-driven processes. Thus, tectonics is commonly responsible for rock—and surface—uplift, while erosion removes part of the emerging relief (e.g. Burbank and Anderson, 2011; Keller and Pinter, 2002; Whittaker, 2012). The final result depends on the balance between long-term erosional and tectonic rates. In active and recent orogens, steep topography and exhumed deep-seated rocks usually witness fast denudation processes concomitant with high uplift rates. On the contrary, present-day exhumed old orogens (Paleozoic and older) generally represent a longer and protracted history with several reactivation episodes of alternating burial and denudation.

Geochronology has become an essential tool to decipher orogenic evolution in general and exhumation histories in particular. Different chronometers provide information on different moments of the PT path undergone by a rock. Those systems with high closure temperatures (e.g. U–Pb on zircon) yield information on the deeper portions of the exhumation PT path, which is often exclusively controlled by tectonic and magmatic processes. The shallower part of the PT path can be investigated through low temperature geochronology, being usually controlled by both tectonic (faulting and folding) and erosional processes. Low temperature geochronology has been extensively applied to recent and active orogens (e.g. Kali et al., 2010; Kirstein et al., 2010; Vázquez et al., 2011), where Neogene–Quaternary basins also provide a time frame for the final exhumation of metamorphic

* Corresponding author.
E-mail address: jabaloy@ugr.es (A. Jabaloy-Sánchez).

http://dx.doi.org/10.1016/j.tecto.2015.06.034
0040-1951/

terranes. Older orogens have received less attention regarding its recent thermal and exhumation history (e.g. Kohn et al., 2002; Miller et al., 2013), assuming that generally those regions were exhumed during the vanishing stages of the corresponding orogeny.

The post-Paleozoic vertical movements of the SW Iberian Variscides are poorly known mainly due to the scarce low-temperature geochronological data available and the nearly absence of post-Paleozoic sediments. However, those data point to a complicated evolution of the region, with exhumation occurred at Triassic–Early Jurassic times in a rifting episode related to Pangea break-up (Stapel, 1999; Barbero and López-Garrido, 2006; Juez-Larré and Ter Voorde, 2009, and references therein). These ages contrast with the fact that local relief in the Sierra Morena can reach 500 m and streams show V-shaped deep incised valleys, which point to recent tectonic—and exhumation—activity. This recent uplift of the Sierra Morena was interpreted as due to lithospheric folding (e.g. Cloetingh et al., 2002; Fernández-Lozano et al., 2012; Tejero et al., 2010).

Our work in the SW Iberian Variscides provides new low-temperature geochronological data, namely apatite fission-track and apatite (U–Th)/He cooling ages on samples from Variscan and pre-Variscan granitoids, which serve to feature time–temperature paths, as well as to constrain the post-Paleozoic thermal and exhumation evolution of this region.

2. Geological setting

The Iberian Massif (Fig. 1a) constitutes the most complete transect of the Late Paleozoic Variscan Orogen (e.g. Simancas et al., 2013), whose outcrop extends to the South in NW Africa and to the North in France and Central Europe. The Variscides have a counterpart in North America, namely the Alleghanides, which crop out in the Appalachian and Ouachita Mountains. The Variscan–Alleghanian orogenic system resulted from the complex collision in Late Paleozoic times of two continental plates, Gondwana and Laurussia, after the consumption of the Rheic Ocean (e.g. Kroner and Romer, 2013; Matte, 2001). As a whole, the Iberian Variscides feature an S-shaped orocline (Martínez-Catalán, 2011, 2012; Shaw et al., 2012), whose final development seems to have occurred in Early Permian times (Weil et al., 2000) and marks the end of the Variscan orogeny.

The Iberian Massif has been classically divided into a number of zones (Fig. 1a) according to stratigraphic, tectonic, metamorphic and magmatic criteria (e.g. Julivert et al., 1972; Lotze, 1945). A detailed description of these zones is beyond the scope of this paper. Thus, we will present a brief summary of this zoning and its interpretation. In the Northern Iberian Massif, the Cantabrian zone constitutes the most external zone, being characterized by thin-skinned tectonics developed on the passive margin Paleozoic sediments of Gondwana (e.g. Pérez-Estaún et al., 1988). Westward from the Cantabrian Zone, the West Asturian Leonese Zone and the Central Iberian Zone represent progressively more internal domains affected by ductile deformation and low- to medium-grade metamorphism. Finally, the Galicia Tras-Os-Montes Zone appears as an allochthonous—and exotic to Gondwana—domain with continental and oceanic units (e.g. Martínez-Catalán et al., 1996).

In the southwestern Iberian Massif (Fig. 1b), the South Portuguese Zone is the most external one, having been affected by thin-skinned tectonics developed on Devonian to Lower Carboniferous sedimentary rocks, generally attributed to Avalonia (a palaeogeographic domain linked to Laurussia). Northwards, the Ossa-Morena Zone and the Central Iberian Zone represent the hinterland, with penetrative ductile deformations and variable metamorphism. The boundary between the South Portuguese and the Ossa-Morena Zone is generally interpreted as the Rheic suture, while the Ossa-Morena/Central Iberian contact seems to correspond to a lesser-scale suture, attesting the closure of a narrow ocean (Gómez-Pugnaire et al., 2003; Simancas et al., 2013).

Apart from the pre-Variscan magmatic bodies, the Paleozoic sequences of the southwestern Iberian Massif contain intrusive complexes mainly with tonalitic to granitic compositions and intrusion ages ranging from ≈350 to 300 Ma (e.g. El Hadi et al., 2006; Simancas et al., 2013).

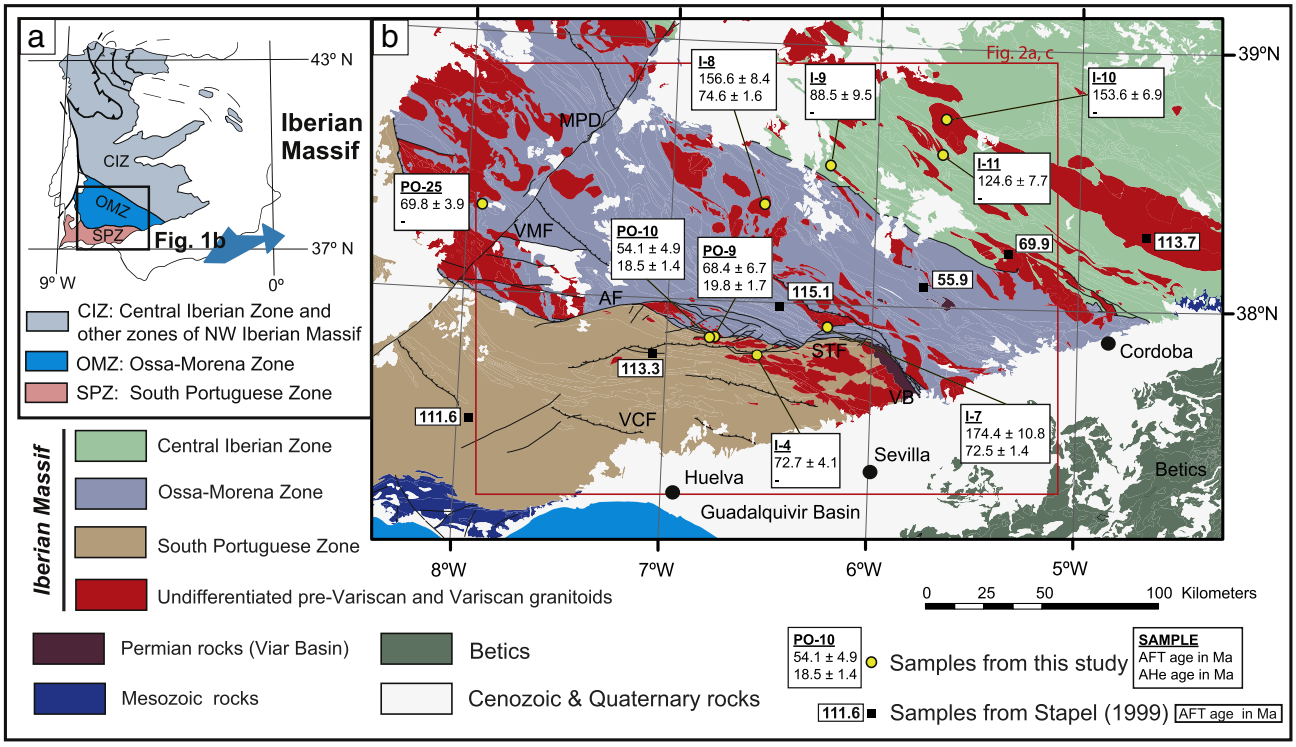

Fig 1. (a) Location of the study area (rectangle) within the Iberian Massif. (b) Geological sketch of the SW Iberian Variscides showing the location of the granitoids sampled in our low-temperature geochronological work (yellow circles) and their AFT and AHe ages. The location and AFT ages of the samples from Stapel (1999) are also marked in black squares. Acronyms: AF: Aroche Fault, MPD: Messejana-Plasencia Dyke, STF: San Telmo Fault, VMF: Vidigueira–Moura Fault, VCF: Villanueva de los Castillejos Fault.

The Lower Permian continental deposits from the Viar Basin (Fig. 1b) contain abundant Autunian flora (Broutin, 1981) and cover unconformably the rocks at the boundary between the South Portuguese and the Ossa-Morena Zone (Simancas, 1983). Finally, Late Cretaceous (88.3 ± 0.5 Ma and 68.8 ± 1.0 Ma; Grange et al., 2010) alkaline igneous rocks outcrop in central and southern Portugal (Sintra, Sines, Monchique).

3. Tectonic geomorphology of the SW Iberian Variscides

Most of the Iberian massif is dominated by a ≈600 m high plateau (Iberian Meseta) surrounded by Alpine mountain ranges to the North (Cantabrian Mountains), the East (Iberian ranges) and South (Sierra Morena and Betic ranges). The Iberian Meseta is interrupted by the Alpine Central System, which reaches altitudes of 2000 m. This topography is indicative of a certain grade of tectonic activity in Alpine times, concentrated in the margins and the center of the Iberian Meseta. According to geomorphic criteria, the Iberian Meseta features plains at different elevations, which, as a whole, are interpreted as the remains of a large polygenic erosional surface that truncates the Variscan basement (Birot and Solé Sabarís, 1954; Tejero et al., 2010) and formed at Late Cretaceous–Early Paleogene times (Feio, 1951; Ferreira, 1980; Martín-Serrano, 1988; Cabral, 1995).

Despite the aforementioned erosional surface, the prominent relief of the SW Iberian Massif denotes some degree of Alpine tectonic activity. Thus, the topography of this region consists in an ENE–WSW trending mountainous region, namely the Sierra Morena, with average elevations progressively decreasing westward from ≈1300 to ≈200 m.a.s.l. (Fig. 2a). To the South, the Sierra Morena is bounded by a sharp ENE–WSW oriented topographic escarpment, which separates the mountainous area from the flat Guadalquivir valley (Figs. 1b and 2). This flat region constitutes the foreland basin of the Betic Cordillera located to the South. To the North, the relief of the Sierra Morena decreases, progressively joining the Iberian Meseta.

The drainage network in the southern slopes of Sierra Morena is dominated by NW–SE oriented streams, which are tributaries of the Guadalquivir River (Fig. 2a). In the western Sierra Morena, three main rivers, namely Tinto, Odiel, and Guadiana, cut through the relief with N–S trend, directly flowing to the Atlantic Ocean (Fig. 2a). Some Cenozoic faults have been described, as the Vidigueira–Moura (VMF in Figs. 1 and 2), the Guadalupe–Montánchez, and the northern Badajoz basin faults; these faults are north-dipping surfaces with reverse left-lateral regimes, giving way to vertical throws of hundreds of meters to 1 km (Álvarez et al., 2004; Brum da Silveira et al., 2009). The footwall blocks of these faults appear covered by Cenozoic continental sedimentary rocks deposited during faulting.

Apart from the abovementioned Alpine faults, other faults with inferred Alpine activity can be recognized in the Variscan outcrops drawing on their topographic expressions. The western Sierra Morena slope map shows, from south to north, a first escarpment located at Villanueva de los Castillejos, where a plain area to the south is cut by a WNW–ESE trending mountain front (Figs. 2 and 3a and b). This escarpment is approximately 150 m-high and coincides with the trace of the north dipping Villanueva de los Castillejos thrust fault, which superposes Early Carboniferous rocks with different ages, but with roughly the same strengths. To the north, a second escarpment, namely San Telmo Fault, with E–W orientation and ≈500 m-high is located south of Aracena (Figs. 2 and 3c). A third topographic step with 250 m of local relief and E–W orientation is located north of Aroche (Fig. 2), in close coincidence with the so-called Beja-Valdelarco (Apalategui et al., 1983) or Aroche Fault (Simancas et al., 2003).

Other expressions of Alpine or recent tectonics in the area come from the presence of some waterfalls along the Guadiana river and its tributaries, in places with homogenous lithologies in terms of strength and erodibility. Thus, the main rivers of the Guadiana fluvial system show topographic steps that concentrate mainly in the low and middle courses of the trunk river. In its low course, the Guadiana River is entrenched in a narrow gorge (Guadiana canyon) with steep slopes at both sides (Figs. 2 and 3d). The entrenchment is around 50–60 m when cutting through the Pulo do Lobo unit, where a 20 m-high fall is observed (Fig. 3e). This fall is located on a monotonous sequence of phyllites and quartzites, the so-called Pulo do Lobo Formation, without strong lithological contrasts. Downstream from the fall, the Guadiana River presents a transversal profile with strath terraces at 20 m over the water channel (Fig. 3f).

4. Apatite (U–Th)/He and fission-track determinations

4.1. Samples and methods

In order to determinate the Mesozoic–Cenozoic thermal history of SW Iberian Massif, we have combined AFT and AHe analyses. To do so, we collected 35 samples, though only nine of them contained sufficient high-quality apatite grains as to perform the thermochronological analysis. Thus, we have determined nine AFT ages and five AHe ages (Tables 1 and 2).

In the southern Sierra Morena, five AFT ages (I-4, I-7, PO-9, PO-10, and PO-25) and three AHe ages (I-7, PO-10, and PO-9) were obtained (Figs. 1b and 2a). These samples were collected from various igneous and metaigneous bodies:

a) Sierra Norte de Sevilla monzogranite (I-4). Zircons from this sample yield a SHRIMP U–Pb age of 344 ± 3 Ma (Pérez-Cáceres, pers. comm.).
b) Santa Olalla del Cala granodiorite (I-7), with an age of 347 ± 3.4 Ma determined by SHRIMP-zircon U–Pb dating (Ordóñez-Casado et al., 2008).
c) Beja-Acebuches amphibolites (samples PO-9 and PO-10). Zircons from one of these samples (PO-10) yielded a SHRIMP U–Pb protolith age of 332 ± 3 Ma (Azor et al., 2008).
d) Viana do Alentejo orthogneiss (PO-25), with a protolith age of ≈600 Ma according to SHRIMP-zircon U–Pb dating (Martínez-Poyatos, pers. comm.).

Sample I-4 is located in the footwall of the reverse San Telmo fault, while samples I-7, PO-9, and PO-10 are in the hanging-wall of this fault (Fig. 2). Sample PO-25 is located in the hanging wall of the Vidigueira–Moura fault (Fig. 1).

Two more samples from the central Sierra Morena were studied, namely a granodiorite from the Burguillos del Cerro pluton (sample I-8, dated at 338 ± 1.5 Ma by the conventional U–Pb method on zircon grains; Casquet et al., 2001), and a metagranite from the Ribera del Fresno orthogneiss (I-9, with a protolith age of 475 ± 7 Ma obtained by SHRIMP-zircon U–Pb dating; Schäfer, 1990).

Finally, the northern Sierra Morena was sampled at Los Pedroches granodiorite (I-10, with an age of 307.7 ± 0.4 Ma obtained by conventional U–Pb zircon dating; Carracedo et al., 2009) and Valle de la Serena orthogneiss (I-11, with a protolith age of 573 ± 14 Ma obtained by SHRIMP-zircon U–Pb dating; Ordóñez-Casado, 1998).

Apatite grains were separated using standard heavy-liquid and magnetic techniques. To perform fission track analysis on apatite, aliquots were mounted in epoxy, polished to expose internal crystal surfaces, and etched with 5.5 M HNO_3 during 18 to 20 s at 20 ± 0.5 °C. Low-U muscovite sheets were fixed to the mounts, to be used as external detectors, and samples were irradiated in the FRM II Research Reactor at the Technische Universität München (Germany). Apatite samples were irradiated together with IRMM 540R dosimeter glasses and Durango and Fish Canyon Tuff age standards. After irradiation, the mica detectors of all samples and standards were etched with 48% HF during 40 min at room temperature. The samples and standards were counted dry at 1250× magnification, using a Carl Zeiss Axio Imager M1m optical microscope and the FTStage 4.04 system. Apatite

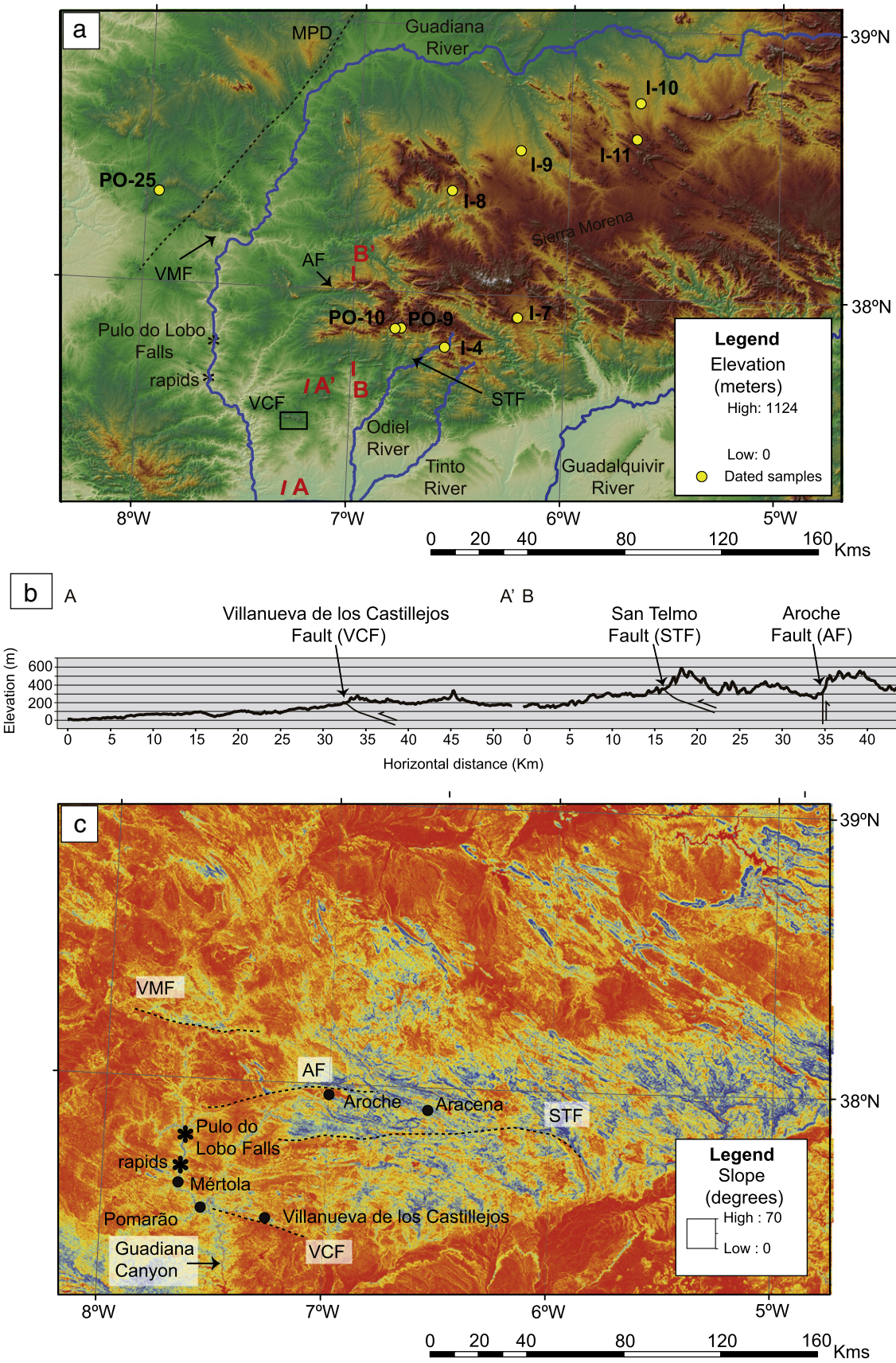

Fig 2. (a) Hypsometric map of the western Sierra Morena with location of the main topographic escarpments attributed to Alpine fault activity (AF, STF and VCF). AA′ and BB′ locate the composite topographic profile shown in b. Yellow circles locate the samples used for the geochronological study. Acronyms as in Fig. 1b. (b) Composite topographic profile with the location of three major topographic scarps and the related faults. (c) Slope map of the western Sierra Morena with location of the major topographic scarps mentioned in the text. Acronyms as in Fig. 1b.

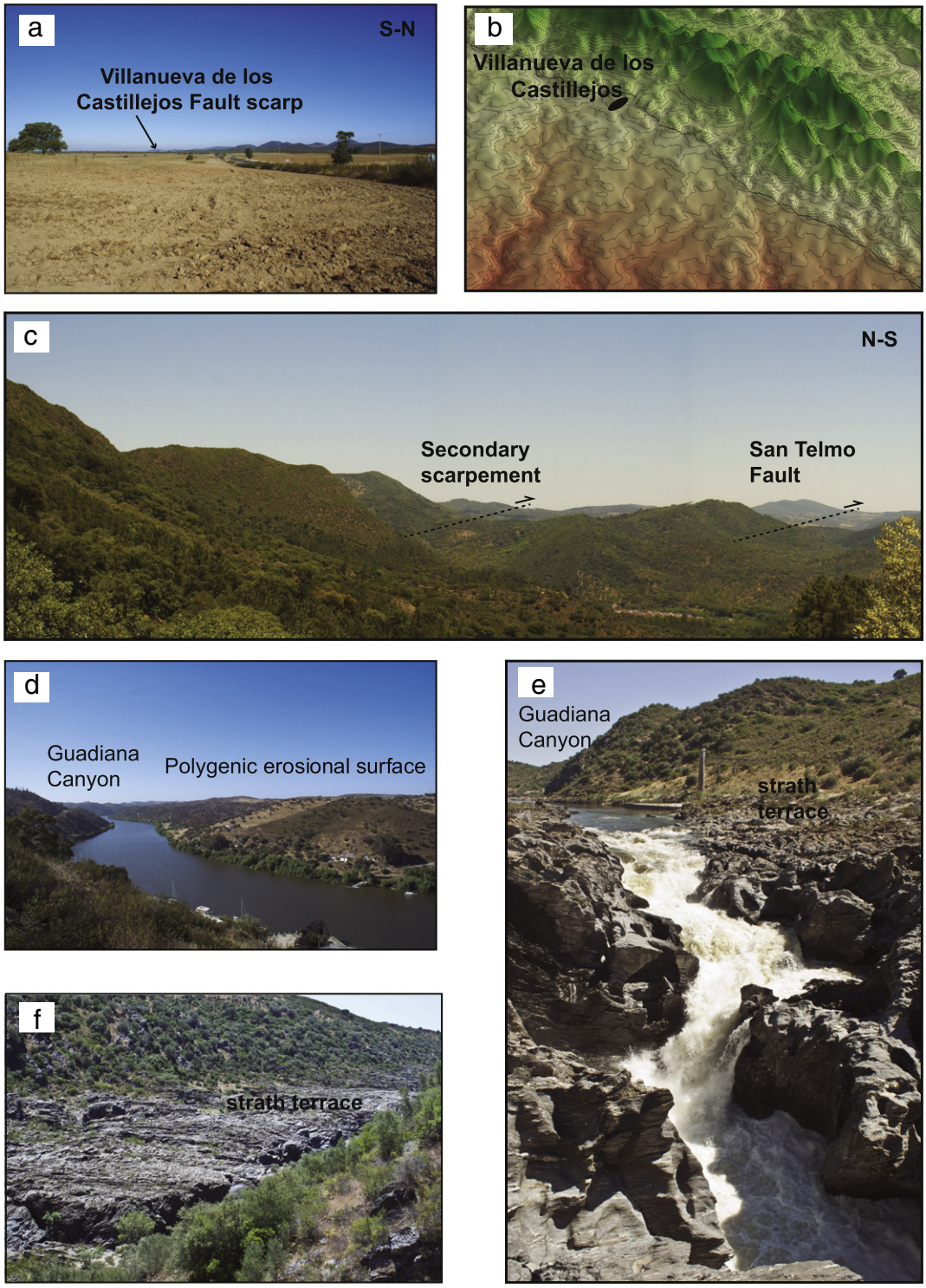

Fig 3. Photographs of the main geomorphic features discussed in the text. (a) Topographic escarpment of Villanueva de los Castillejos viewed from the east. (b) Oblique aerial view of the Villanueva de los Castillejos escarpment obtained with ArcScene (see Fig. 2a and c for location). (c) View from the west of San Telmo Fault topographic escarpment (westwards of Aracena). (d) View at Pomarão (Portugal) of the Guadiana River channel entrenched into the so-called polygenic erosional surface (see Fig. 2a and c for location). (e, f) Views of the Pulo do Lobo Falls (Portugal) and strath terraces at both sides of the channel.

fission-track ages were calculated applying the ζ-method (external detector method) described by Hurford and Green (1982, 1983). The ζ-value of 337.21 (±13) was obtained by counting several Durango, Fish Canyon and Mont Dromedary apatite age standards (see details in Table 1). The fission track age passes the χ^2 test (Galbraith and Laslett, 1993), thus suggesting that the whole set of individual apatite grain ages in one sample belongs to one homogeneous population (Table 1). We were able to measure a representative number of horizontal confined track lengths and the lengths of etch pits of tracks that crop out on the etched surface (Dpar).

Table 1
Apatite fission track data of samples from the southwestern Iberian Massif.

Sample	Elevation (m)	X (UTM)	Y (UTM)	No. of grains	ρ_D (10^6 cm^{-2}) (N_D)	ρ_s (10^6 cm^{-2}) (N_S)	ρ_i (10^6 cm^{-2}) (N_i)	P (%)	AFT age ($\pm 2\sigma$) (Ma)	Mean track length (μm) (No. of tracks)	SD (μm)	D_{par} (μm)	U (std) (ppm)	Emplacement age
I-4	316	715407	4186565	20	1.28108 (7264)	0.4941 (673)	1.3647 (1859)	58.40	72.7 ± 4.1	13.2 (102)	2.38	2.82 (250)	15.4 (3.2)	344.4 ± 3 Ma (Pérez-Cáceres, pers.comm)
I-7	500	744651	4200525	20	1.28714 (7298)	0.7115 (622)	0.9495 (830)	95.84	174.4 ± 10.8	10.3 (34)	2.71	2.76 (164)	8.8 (1.4)	347 ± 3.4 Ma Ordóñez-Casado et al. (2008)
I-8	451	714526	4251313	20	1.29017 (7315)	0.9612 (974)	1.2257 (1242)	81.39	156.6 ± 8.4	13.9 (78)	2.47	2.63 (273)	13.4 (1.8)	338 ± 1.5 Ma Casquet et al. (2001)
I-9	422	741752	4269626	20	1.29320 (7332)	0.2059 (138)	0.4669 (313)	99.95	88.5 ± 9.5	10.9 (28)	2.96	2.69 (229)	5.4 (1.9)	475 ± 7 Ma Schäfer (1990)
I-10	423	268303	4290335	20	1.29623 (7350)	2. 2060 (1697)	2.8481 (2392)	70.74	153.6 ± 6.9	12.9 (103)	2.56	2.81 (210)	29.4 (9.7)	307.7 ± 0.4 Ma Ordóñez-Casado et al. (2008)
I-11	552	266758	4275337	20	1.29926 (7367)	0.897 (567)	1.5615 (987)	94.33	124.6 ± 7.7	10.9 (20)	2.80	2.73 (191)	15.8 (5.1)	573 ± 14 Ma Ordóñez-Casado (1998)
PO-9	542	696860	4193170	20	1.30229 (7384)	0.2241 (161)	0.6612 (475)	49.58	68.4 ± 6.7	13.5 (82)	2.44	2.78 (171)	7.8 (2.9)	340–332 Ma Azor et al. (2008)
PO-10	559	694428	4192721	20	1.30532 (7401)	0.269 (179)	1.0838 (701)	77.20	54.1 ± 4.9	12.4 (82)	2.80	2.81 (195)	11.7 (4.1)	332 ± 3 Ma Azor et al. (2008)
PO-25	220	593650	4243474	20	1.30835 (7418)	0.9942 (608)	3.1037 (1898)	70.70	69.8 ± 3.9	12.3 (56)	2.89	2.77 (200)	33.2 (11.9)	595–593 Ma

Martínez-Poyatos,pers.comm)ρ_D: track density on the mica sheets adjacent to the glass dosimeters during irradiation; ρ_s: spontaneous track density; N_s: number of counted spontaneous tracks; ρ_i: induced track density; N_i: number of counted induced tracks; P (%): probability that all grains belong to the same population.
AFT ages are calculated using a ζ (MV) value of 337 ± 13 for dosimeter IRMM-540R standard glass. The ζ (MV) value was obtained after measured 22 apatite standards (Durango, Fish Canyon and Mont Dromedary) in the Low-Temperature Thermochronology Laboratory at the School of Geographical and Earth Sciences, University of Glasgow (UK).
Measured value of ρ_s was multiplied by a geometry factor of 0.5 to calculate the AFT ages.

The AHe analyses were performed at SUERC (Glasgow). Individual crystals were hand-picked under a binocular microscope at 218× magnification. Crystal dimensions were measured with a calibrated graticule. One or two grains were loaded into standard Pt foil tubes and analyzed using standard procedures (Foeken et al., 2006). The alpha-emission correction (Ft) is based on emission from all surfaces (Balestrieri et al., 2005) (see Table 2 for details). The results in Table 2 come from three or four replicates of each sample. Uncertainty in the ages obtained is 10% ($\pm 1\sigma$) based on laboratory reproducibility. Sample I-10 does not show a positive relationship between grain size and uncorrected He ages. Therefore, the age variation might be an artifact due to unobserved U-, Th- and or He-bearing inclusions. For this reason, we do not use this AHe age in our regional interpretation.

Modeling of AFT and AHe thermal histories was performed using the HeFTy software (Ketcham, 2005). Cooling histories were determined using the multi-kinetic AFT annealing model of Ketcham et al. (2007) for etching conditions of 5.5 M HNO_3. Single grain-age counting data and track-length measurements were incorporated in the model and combined with the Dpars as kinetic parameter. C-axis track length projection (Ketcham et al., 1999) has been used. AFT and AHe data were modeled together. For the AHe data, we have used the value of each single grain analyses, including single ages, grains radius and U and Th concentrations. We have used the Flowers et al. (2009) algorithm to determine He diffusion. Furthermore, we have incorporated two external constraints (Table 1): 1) a box to allow high temperatures (>600 °C) conditions following the emplacement age of the granitoids studied, and 2) in the case of the samples coming from the southern Sierra Morena, another box to allow the rocks to be at surface temperatures at Early Permian time, as it is shown by the fact that clasts of the Paleozoic sequence were incorporated into the sediments of that age in the Viar Basin (Broutin, 1981; Simancas, 1983). However this second constraint cannot be applied to the samples of the central and northern Sierra Morena, since no Permian sediments crop out there. HeFTy software produces a large number of time-temperature paths (in our case 50,000). The AFT and AHe predicted data are then compared to the measured values and only those time-temperature paths with good or acceptable fit are retained.

Fig. 4 provides a graphic summary of representative models of thermal histories for different samples across the SW Iberian Massif. For each sample, the green and purple areas depict statistically acceptable and good fit paths, respectively, with thick lines corresponding to the best fit thermal histories. The goodness-of-fit (GOF) provides a numerical value representative of the fit between observed and predicted values (values close to 1 are the best; a value >0.5 is considered good; a value >0.05 is considered acceptable) (Table 1).

4.2. Results

The determined AFT ages are oldest than AHe ages in all cases. As a whole, AFT ages vary between 54.1 ± 4.9 and 174.4 ± 10.8, though most of them range from 54.1 ± 4.9 to 72.7 ± 4.1 Ma. No clear correlation between AFT ages and elevation is observed. Mean track length (MTL) varies from 10.5 to 12.5 μm. D_{par} values range from 2.6 to 2.8 μm, indicating that the apatite grains studied show annealing features similar to those of the Durango apatite. AHe of multiple aliquots replicate well, with the exception of the sample PO-9 (Table 1). Individual AHe ages range from 14.0 ± 1.0 to 88.6 ± 1.5 Ma, showing a negative correlation with elevation.

The interpretation of apatite (U–Th)/He data has been performed by taking into account the accumulation of crystal defects. To do so, the effective uranium factor (eU) has been considered by applying the expression eU = [U] + 0.235 [Th] (Table 2), where [U] and [Th] are ppm concentrations of U and Th in the apatite crystals. This factor characterizes the dependency of ^{4}He-diffusion on the amount of accumulated crystal defects created by the movements of the fission products and the alpha-recoil nucleus in the crystal lattice. The eU values of sample

Table 2
Apatite (U–Th)/He data and information from samples from the southwestern Iberian Massif.

Sample	^{4}He (fml)	^{238}U (ppm)	^{232}Th (ppm)	eU	Number crystals	Equivalent radius (μm)*	Uncorrected He age (Ma)	Corrected He age (Ma)†	Mean ages (Ma)
I-7	377	6.3	11.9	9.1	2	145	80.5	88.6 ± 1.5	72.5 ± 1.4
	189	15.3	20.5	20.1	2	95	62.9	73.0 ± 1.2	
	54	14.0	9.1	16.1	2	78	46.1	55.8 ± 1.4	
I-8	64	14.5	47.2	25.6	2	54	65.8	85.0 ± 1.7	74.6 ± 1.6
	58	23.7	87.9	44.4	2	37	49.6	70.4 ± 1.3	
	30	10.9	37.5	19.7	2	57	52.4	68.4 ± 1.7	
I-10	255	64.2	97.4	87.1	2	45	102.4	138 ± 2.4	138.6 ± 2.5
	392	86.4	126.7	116.1	2	49	114.4	152 ± 2.6	
	112	83.3	118.2	111.1	2	35	87.2	132 ± 2.6	
PO-10	3	7.6	27.6	14.1	2	46	14.3	19.9 ± 1.7	18.5 ± 1.4
	3	13.6	40.3	23.1	2	40	9.7	14.0 ± 1.0	
	8	4.2	68.2	20.2	2	46	16.4	21.9 ± 0.8	
	2	6.8	38.7	15.8	2	37	12.4	18.2 ± 2.0	
PO-9	12	9.3	24.1	15.0	2	50	32.9	45.7 ± 1.6	19.8 ± 1.7
	3	11.5	31.1	18.8	2	42	13.9	21.3 ± 1.6	
	2	18.7	48.2	30.1	2	48	3.4	4.6 ± 0.4	
	5	17.1	96.9	39.9	2	31	20.1	33.6 ± 3.2	

* The equivalent radius is the radius of a sphere with a surface to volume ratio equal to the apatite crystal.
† Alpha emission correction for broken grains assumes that broken faces represent zero-loss. F_t is increased by a factor equal to the ratio of the total grain surface area of the assumed emitting faces. This typically increases F_t by <10%. No systematic relationship between the fraction of broken grains and corrected ages has been observed indicating that the correction method is robust.

I-10 (87–116 ppm) are significantly higher than those of the other samples (9–44 ppm). This high eU factor could explain why sample I-10 shows the older AHe age (138.6 ± 2.5), which is very close to the corresponding AFT (153.6 ± 2.5). No paths were found when AFT and AHe data from this sample were modeled together. The implantation from external phases, microinclusions with high eU, and fluid inclusions could induce the anomalously old (U–Th)/He dates in sample I-10. For this reason, we do not use the AHe age from sample I-10 in our regional interpretation.

The oldest ages have been obtained for sample I-7 in southern Sierra Morena, with an AFT age of 174.4 ± 10.8 Ma and a mean AHe age of 72.5 ± 1.4 Ma. We have only modeled the thermal history of those samples with an adequate amount of measured track lengths (samples I-4, I-8, I-10, PO-9, PO-10, and PO-25; Fig. 4). Finally, to convert cooling rates to denudation rates during Late Cenozoic times we have used geothermal gradients ranging from 19 to 29 °C km^{-1}, in accordance with the values provided by Fernàndez et al. (1998) for SW Iberia.

The obtained time–temperature paths for the samples from the southern and central Sierra Morena show a similar evolution during Mesozoic and Cenozoic times, characterized by a rapid cooling beginning at ≈20 Ma in most of them (Fig. 4a, c, and d). Thus, samples I-4, PO-10 and PO-25 show cooling rates between 3.2 and 3.6 °C Ma^{-1} for the last 20 Ma, which, in turn, correspond to denudation rates of 0.110 to 0.189 mm year^{-1}. Finally, sample PO-9 shows a less constrained recent cooling, probably due to the dispersion of the AHe ages. Nevertheless, this sample also depicts a rapid cooling event starting at 35 Ma (Fig. 4b) at 2.7 °C Ma^{-1}, with estimated denudation rates varying between 0.093 and 0.142 mm year^{-1}.

The obtained time-temperature paths for the northern Sierra Morena samples are slightly different. In this case, a rapid cooling stage beginning at ≈70 Ma (Fig. 4e and f) is deduced from the modeling. Sample I-8 has an AFT age of 156.6 ± 8.4 Ma and a mean AHe age of 74.6 ± 1.6 Ma, depicting a long time-span with little or no cooling (flat section between ~190 and ~100 Ma; Fig. 4e), which is consistent with a very low rate of exhumation for that period; at ≈100 Ma, the cooling rate shows a remarkable increase (2–2.5 °C Ma^{-1}), reaching surface temperatures at ≈50 Ma. AFT ages of samples I-10 and I-11 are 124.6 ± 7.7 (I-11) and 153.6 ± 6.9 (I-10) Ma. Time–temperature path of sample I-10 indicates a long interval with little or no cooling (flat section in the corresponding diagram of Fig.4f) that is consistent with a very low rate of exhumation until ~80 Ma. From 80 Ma onwards, cooling and exhumation rates increase significantly (1.14 °C Ma^{-1} and 0.039 to 0.060 mm year^{-1}).

5. Discussion and conclusions

The Mesozoic and Cenozoic thermal histories determined from AFT and AHe ages for the SW Iberian Variscides attest an Early Mesozoic heating episode that reset the AFT ages. This Early Mesozoic heating was followed by several Mesozoic fast cooling stages alternating with long episodes with little or no cooling. Cooling and exhumation lasted until Alpine times, since some samples show thermal histories with rapid cooling at Cenozoic times.

5.1. Mesozoic cooling/exhumation stages

An important heating stage occurred in Triassic–Early Jurassic times, being responsible for the complete annealing of previous AFT. Our data suggest that this heating episode ended between 210 and 160 Ma and was followed by a cooling event. This Early Mesozoic thermal episode was recorded by different thermochronometers in most of the Iberian Peninsula (see Juez-Larré and Ter Voorde, 2009, and references therein). These authors indicate that this Triassic–Early Jurassic thermal stage can be the responsible for the lack of cooling ages older than 200 Ma. This stage coincided with the breakup of Pangea and the onset of the rifting that gave way to the Atlantic Ocean, having been also recorded in other sectors of the central and northern Iberian Massif (Barbero et al., 2005; Grobe et al., 2010; Martín-González et al., 2012). Actually, rifting in this stage occurred in the central Atlantic realm, with emplacement of serpentinized mantle rocks overlain by decompression melting basalts and gabbros (e.g. Marzoli et al., 1999; Sibuet et al., 2012; Wilson, 1997). In the Iberian Peninsula, the intrusion of the 500 km-long Messejana-Plasencia dyke (Figs. 1 and 2) at 200 Ma (Cebriá et al., 2003) is attributed to this stage of central Atlantic opening. In the same way, this initial Atlantic rifting was also recorded in the sedimentary sequence of the Lusitanian basin (Rasmussen et al., 1998) west of the Sierra Morena. A cooling stage attested by the AFT cooling age of the sample I-7 (174.4 ± 10.8 Ma, Early Jurassic time), followed the previous registered Triassic–Early Jurassic heating episode. Interestingly, Barbero and López-Garrido (2006) proposed a roughly similar thermal evolution for the southeastern corner of the Iberian Massif, though the estimated AFT cooling ages are older than the Triassic, thus indicating

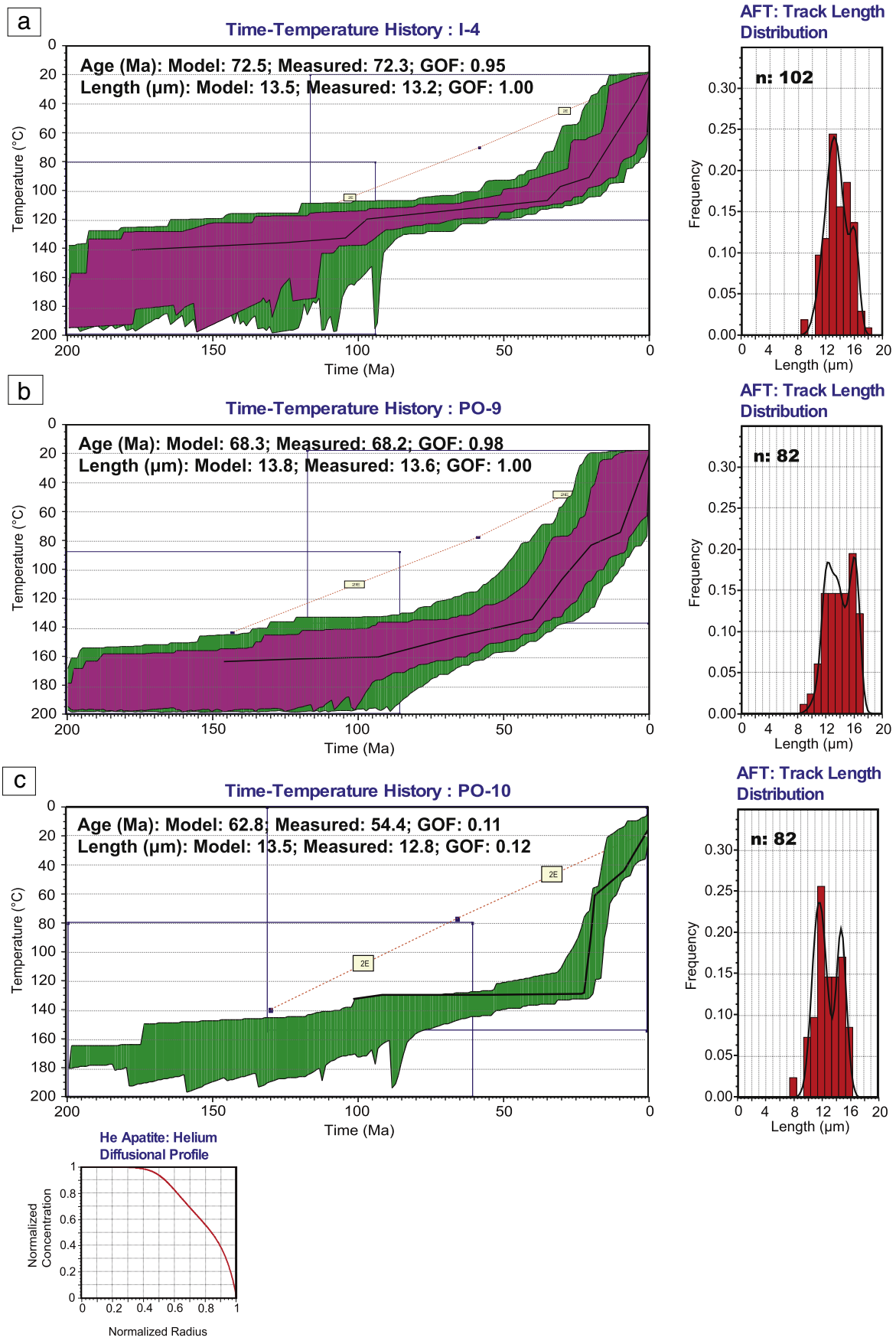
a
Time-Temperature History : I-4
Age (Ma): Model: 72.5; Measured: 72.3; GOF: 0.95
Length (μm): Model: 13.5; Measured: 13.2; GOF: 1.00
Temperature (°C)
Time (Ma)
AFT: Track Length Distribution
n: 102
Frequency
Length (μm)
b
Time-Temperature History : PO-9
Age (Ma): Model: 68.3; Measured: 68.2; GOF: 0.98
Length (μm): Model: 13.8; Measured: 13.6; GOF: 1.00
Temperature (°C)
Time (Ma)
AFT: Track Length Distribution
n: 82
Frequency
Length (μm)
c
Time-Temperature History : PO-10
Age (Ma): Model: 62.8; Measured: 54.4; GOF: 0.11
Length (μm): Model: 13.5; Measured: 12.8; GOF: 0.12
2E
Temperature (°C)
Time (Ma)
AFT: Track Length Distribution
n: 82
Frequency
Length (μm)
He Apatite: Helium Diffusional Profile
Normalized Concentration
Normalized Radius

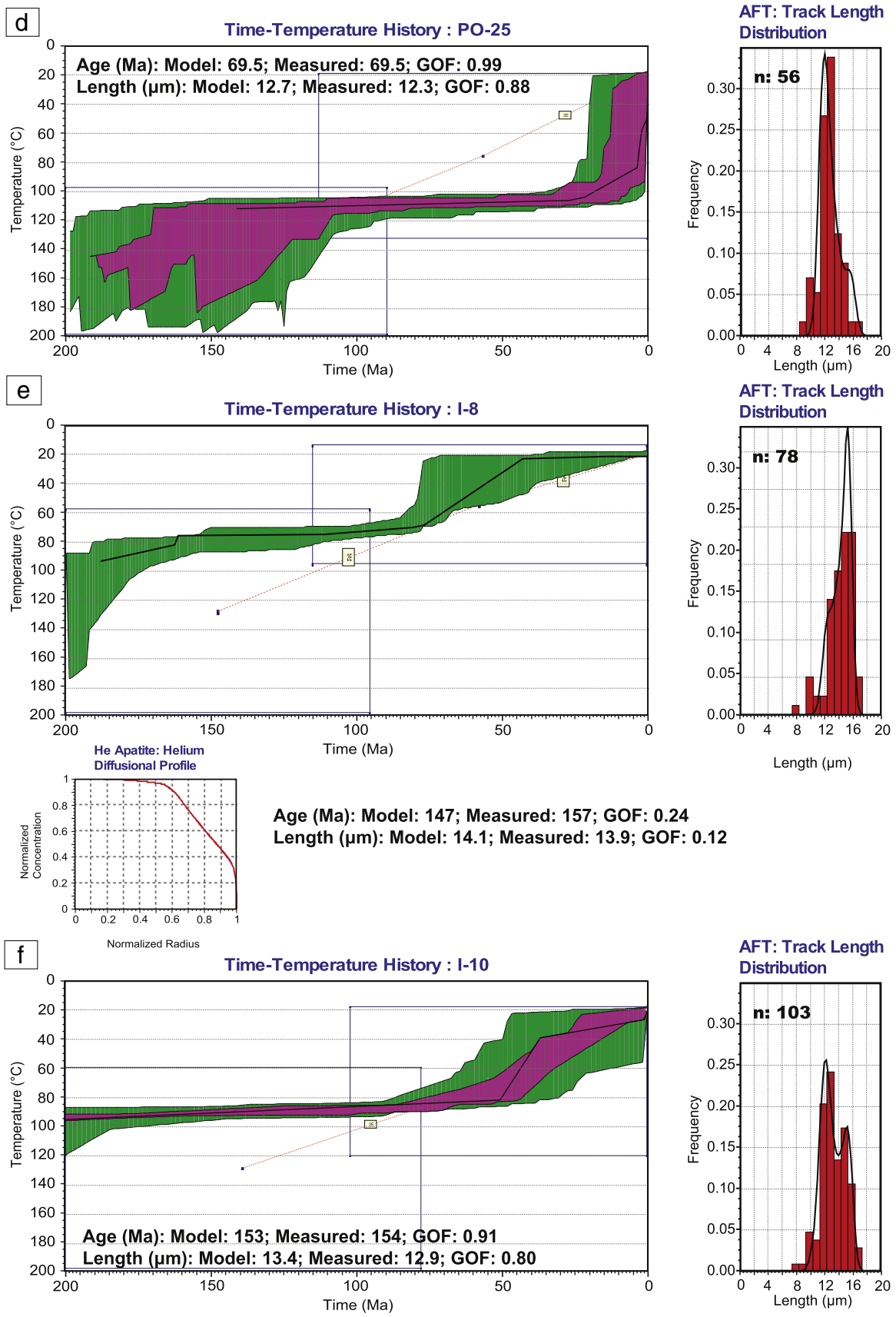

Fig 4. Time–temperature paths obtained from inverse modeling with the HeFTy software (Ketcham, 2005) for samples I-4 (a), PO-9 (b), PO-10 (c), PO-25 (d), I-8 (e), and I-10 (f). This software generates possible T–t paths using a Monte Carlo algorithm. Predicted apatite fission-track data were calculated according to the Ketcham et al. (2007) annealing model and Dpars as kinetic parameter. Mean track lengths are reported after c-axis projection and, therefore, can differ from those listed in Table 1. Age of emplacement of the igneous protoliths and Early Permian exhumation (PO-9, PO-10, PO-25, I-4) converted into time–temperature boxes have been used as constraints.

that these rocks never entered the Complete Annealing Zone of apatite (T > 110 °C). The different temperatures reached along the southern Iberian Massif during the Triassic–Early Jurassic rifting could be due to a higher thermal input at the Atlantic margin (western Iberian Massif) with respect to the Neo-Tethys one (eastern corner of the Iberian Massif).

A second cooling stage in SW Iberia occurred at Late Jurassic–Early Cretaceous times (see Tritlla and Solé, 1999; Juez-Larré and Ter Voorde, 2009, and references therein), and is recorded by the AFT ages of samples I-10 (153.6 ± 6.9 Ma) and I-11 (124.6 ± 7.7 Ma). During this stage, the progression of the Atlantic rifting produced the separation of Newfoundland from Iberia, the emplacement of serpentinized mantle in the West Galician margin (e.g. Schärer et al., 1995; Tucholke et al., 2007), and finally seafloor spreading in the North Atlantic region (Rasmussen et al., 1998).

The aforementioned cooling stages can be interpreted as due to the formation of important marginal rift reliefs, which, in turn, have been related at depth to lithospheric thermal doming (Barbero and López-Garrido, 2006). Thus, rift shoulder erosion would have yielded the large volume of clastic sediments deposited in the Lusitanian basin at Late Jurassic times (Kullberg, 2000; Rasmussen et al., 1998). Furthermore, the variation of cooling ages in small distances (see also Stapel, 1999) suggests that areas experiencing exhumation were relatively small and changed through time, which, in turn, is in agreement with the migration of the locus of extension in the Alentejo margin along the Mesozoic (Pereira and Alves, 2011).

The youngest Mesozoic cooling stage occurred at Late Cretaceous times and is recorded by the ATF ages between 95 and 60 Ma, and the T–t paths of the samples from the northern Sierra Morena (I-8 and I-10). These T–t paths include a cooling stage beginning at ≈80 Ma.

This thermal event was also recognized by Stapel (1999) in a WSW–ENE AFT profile along the Sierra Morena crest between Seville and Córdoba (Fig. 1). This author obtained AFT ages between 56 and 70 Ma for this sector and interpreted them as a local thermal anomaly, though he did not provide any plausible explanation. Actually, this event was coeval with the intrusion of Late Cretaceous alkaline igneous rocks in central and southern Portugal (Sintra, Sines, Monchique), between 88.3 ± 0.5 Ma and 68.8 ± 1.0 Ma (Grange et al., 2010). The most important of these intrusions is the Monchique alkaline complex, with a great unexposed volume at shallow depths (González-Castillo et al., 2014) and scarce AFT ages that suggest fast cooling after intrusion (Terrinha et al., 2006). Grange et al. (2010) proposed that these alkaline massifs as a whole are related to a deep-rooted mantle plume. The thermal input from this mantle plume and the associated intrusions would have produced general exhumation in SW Iberia, which, in turn, would be responsible for the Late Cretaceous cooling event recorded by the AFT ages. Actually, a seismic survey in the Alentejo margin shows that Upper Cretaceous sediments are tilted and eroded due to surface uplift coeval with the intrusion of the alkaline massifs (Pereira and Alves, 2011).

On the contrary, in the southeastern corner of the Iberian massif and its Mesozoic palaeomargin (Neo-Tethys), now incorporated into the external zone of the Betic Cordillera, the Late Cretaceous thermal event consist in a regional heating that has been related to subsidence (Barbero and López-Garrido, 2006).

5.2. Cenozoic cooling/exhumation

The relief of the Sierra Morena suggests recent surface uplift and, therefore, some sort of Alpine tectonic activity in the SW Iberian Variscides as already pointed out in some previous studies (e.g., Brum da Silveira et al., 2009; Salvany, 2004). Some of the ages and thermal histories obtained in our study confirm the Cenozoic activity.

Final exhumation of SW Iberia seems to have occurred in Miocene times with tectonic activity concentrated along some of the faults with topographic scarps. Thus, the thermal histories of samples I-4, PO-10, PO-25 record a fast cooling stage beginning at around 20 Ma. Furthermore, despite the fact that sample PO-9 has an AFT age of 68.4 ± 6.7 Ma and individual AHe ages that do not replicate well, it also shows a fast cooling stage beginning at ≈40 Ma. The cooling rates for samples I-4, PO-10, and PO-25 for the last 30 Ma vary between 3.2 and 3.6 °C Ma^{-1}, which corresponds to denudation rates of 0.110 to 0.189 mm $year^{-1}$. In the particular case of the PO-10 sample, located in the hanging wall of the San Telmo Fault, the 18.5 ± 1.4 Ma AHe age indicates that these rocks were exhumed to temperatures <40 °C (AHe retention zone; Wolf et al., 1998) by that age. This fact points to a moderate Miocene activity of the faults with topographic expression in the Ossa-Morena, due to compressional stresses coming from the most external domain of the Betic Cordillera located to the south. In fact, the studied area represents the foreland of the Betic cordillera and, therefore, its relief must be related somehow to rthis Alpine orogeny located to the south (i.e. Cloetingh et al., 2002). Furthermore, thermal histories deduced from AFT data within the external Betic domain also record a cooling episode/exhumation episode of Miocene age (Barbero and López-Garrido, 2006) and related to roughly NW-directed thrusting.

To conclude, Cenozoic exhumation occurred as a result of roughly N–S heterogeneous intraplate compressional tectonics affecting the whole Iberian plate, which, in the particular case of SW Iberia would have concentrated in the upper crust and reactivated some of the Variscan faults rooted in a middle crust decollement. In northern Iberia, AFT ages and geological data point to exhumation related to reverse faulting in Middle Cenozoic times at ≈50 Ma in the Cantabrian Mountains (Grobe et al., 2010) and Galicia (Martín-González et al., 2012). However, in central Iberia AFT ages (de Bruijne and Andriessen, 2000, 2002) and geological data (de Vicente and Muñoz-Martín, 2013) point to a younger exhumation related to reverse faulting in Miocene time.

Acknowledgements

We acknowledge the financial support by research projects CGL-2011-29920, CGL2011-24101, CSD2006-0041 TOPO-IBERIA CONSOLIDER-INGENIO 2010 from the Spanish Ministry of Science and Innovation, and RNM-148 Research Group from the Junta de Andalucía. Constructive and critical reviews by two anonymous reviewers were very welcome and helped to improve the manuscript.

References

Álvarez, J., Muñoz Martín, A., Vegas, R., de Vicente, G., 2004. Las sierras de Guadalupe-Montánchez. In: Vera, J.A. (Ed.), Geología de España. Madrid (Spain), SGE IGME, pp. 629–631.

Apalategui, O., Barranco, E., Contreras, F., Delgado, M., Roldán, F.J., Quesada, C., 1983. Hoja geológica núm. 916 (Aroche). Mapa Geológico de España E. 1:50.000. I.G.M.E Madrid.

Azor, A., Rubatto, D., Simancas, J.F., González Lodeiro, F., Martínez Poyatos, D., Martín Parra, L.M., Matas, J., 2008. Rheic Ocean ophiolitic remnants in southern Iberia questioned by SHRIMP U–Pb zircon ages on the Beja-Acebuches amphibolites. Tectonics 27 (5). http://dx.doi.org/10.1029/2008TC002306.

Balestrieri, M.L., Stuart, F.M., Persano, C., Abbate, E., Bigazzi, G., 2005. Geomorphic development of the escarpment of the Eritrean margin, southern Red Sea from combined apatite fission tracks and U–Th /He thermochronometry. Earth Planet. Sci. Lett. 231, 97–110.

Barbero, L., López-Garrido, A.C., 2006. Mesozoic thermal history of the Prebetic continental margin (southern Spain): constraints from apatite fission-track analysis. Tectonophysics 422, 115–128.

Barbero, L., Glasmacher, U., Villaseca, A.C., García, J.A.L., Martín-Romera, C., 2005. Long-term thermo-tectonic evolution of the Montes de Toledo area (Central Hercynian Belt, Spain): constraints from apatite fission-track analysis. Int. J. Earth Sci. 94, 193–203. http://dx.doi.org/10.1007/s00531-004-0455-y.

Birot, P., Solé Sabarís, L., 1954. Investigaciones sobre la morfología de la Cordillera Central Española. Consejo Superior de Investigaciones Científicas. CSIC, Madrid, Spain, p. 88.

Broutin, J., 1981. Etude paléobotanique et palynologique du passage Carbonifére-Permien dans les basins continentaux du Sud-Est de la Zone d'Ossa-Morena (environs de Guadalcanal, Espagne du Sud). Implications Paléogéographiques et Stratigraphiques. Université Paris (Ph.D. Thesis, 234 pp.).

Brum da Silveira, A., Cabral, J., Perea, H., Ribeiro, A., 2009. Evidence for coupled reverse and normal active faulting in W Iberia: The Vidigueira–Moura and Alqueva faults (SE Portugal). Tectonophysics 474, 184–199.

Burbank, D.W., Anderson, R.S., 2011. Tectonic Geomorphology. 2nd edition. Wiley-Blackwell (472 pp.).
Cabral, J., 1995. Neotectonica em Portugal Continental. Mem. Inst. Geol. Min. 31 (225 pp.).
Carracedo, M., Paquette, J.L., Alonso Olazabal, A., Santos Zalduegui, J.F., García de Madinabeitia, S., Tiepolo, M., Gil Ibarguchi, J.I., 2009. U–Pb dating of granodiorite and granite units of the Los Pedroches batholith. Implications for geodynamic models of the southern Central Iberian Zone (Iberian Massif). Int. J. Earth. Sci. 98, 1609–1624. http://dx.doi.org/10.1007/s00531-008-0317-0.
Casquet, C., Galindo, C.F., Tornos, F., Velasco, F., Canales, A., 2001. The Aguablanca Cu-Ni ore deposit (Extremadura, Spain), a case of synorogenic orthomagmatic mineralization: age and isotope composition of magmas (Sr, Nd) and ore (S). Ore Geol. Rev. 18, 237–250.
Cebriá, J.M., Lopez-Ruiz, J., Doblas, M., Martins, L.T., Munha, J., 2003. Geochemistry of the Early Jurassic Messejana–Plasencia dyke (Portugal–Spain); Implications on the Origin of the Central Atlantic Magmatic Province. J. Petrol. 44, 547–568.
Cloetingh, S., Burov, E., Beekman, F., Andeweg, B., Andriessen, P.A.M., García-Castellanos, D., de Vicente, G., Vegas, R., 2002. Lithospheric folding in Iberia. Tectonics 21, TC 1041. http://dx.doi.org/10.1029/2001TC901031.
de Bruijne, C.H., Andriessen, P.A.M., 2000. Interplay of intraplate tectonics and surface processes in the Sierra de Guadarrama (central Spain) assessed by apatite fission track analysis, erosion and tectonic movements; from measurements to physical modelling. Phys. Chem. Earth 25, 555–563.
de Bruijne, C.H., Andriessen, P.A.M., 2002. Far field effects of Alpine plate tectonism in the Iberian Microplate recorded by fault-related denudation in the Spanish Central System. In: Kohn, B.P., Green, P.F. (Eds.), Low temperature thermochronology; from tectonics to landscape evolution. Tectonophysics 349, pp. 161–184.
de Vicente, G., Muñoz-Martín, A., 2013. The Madrid Basin and the Central System: a tectonostratigraphic analysis from 2D seismic lines. Tectonophysics 602, 259–285. http://dx.doi.org/10.1016/j.tecto.2012.04.003.
El Hadi, H., Simancas, J.F., Tahiri, A., González-Lodeiro, F., Azor, A., Martínez-Poyatos, D., 2006. Comparative review of the Variscan granitoids of Morocco and Iberia: proposal of a broad zonation. Geodin. Acta 19 (2), 103–116.
Feio, M., 1951. A evolução do relevo do Baixo Alentejo e Algarve. Comunicações dos Serviços Geológicos de Portugal XXXII (2ª parte), pp. 303–504.
Fernàndez, M., Marzán, I., Correia, A., Ramalho, E., 1998. Heat flow, heat production, and lithospheric thermal regime in the Iberian Peninsula. Tectonophysics 291, 29–53. http://dx.doi.org/10.1016/S0040-1951(98)00029-8.
Fernández-Lozano, J., Sokoutis, D., Willingshofer, E., Dombrádi, E., Martín, A.M., De Vicente, G., Cloetingh, S., 2012. Integrated gravity and topography analysis in analog models: intraplate deformation in Iberia. Tectonics 31 (6). http://dx.doi.org/10.1029/2012TC003122.
Ferreira, B., 1980. Planation surfaces and neotectonics in the Northern Iberia, Portugal. Revue de Geologie Dynamique et de Geographie Physique 22, pp. 51–62.
Flowers, R.M., Ketchman, R.A., Shuster, D.L., Farley, K.A., 2009. Apatite (U–Th)/He thermochronometry using a radiation damage accumulation and annealing model. Geochim. Cosmochim. Acta 73, 2347–2365.
Foeken, J.P.T., Stuart, F.M., Dobson, K.J., Persano, C., Vilbert, D., 2006. A diode laser system for heating minerals for (U–Th)/He chronometry. Geochem. Geophys. Geosyst. 7, Q04015.
Galbraith, R.F., Laslett, G.M., 1993. Statistical methods for fission track ages. Nucl. Tracks 21, 459–470.
Gómez-Pugnaire, M.T., Azor, A., López-Sánchez Vizcaino, V., Soler, J.M., 2003. The amphibolites from the Ossa-Morena/Central Iberian Variscan suture (southwestern Iberian Massif): geochemistry and tectonic interpretation. Lithos 68, 23–42.
González-Castillo, L., Galindo-Zaldívar, J., Ruiz-Constán, A., Pedrera, A., 2014. Magnetic evidence of a crustal fault affecting a linear laccolith: the Guadiana Fault and the Monchique Alkaline Complex (SW Iberian Peninsula). J. Geodyn. 77, 149–157. http://dx.doi.org/10.1016/j.jog.2013.10.007.
Grange, M., Schärer, U., Merle, R., Girardeau, J., Cornen, G., 2010. Plume-Lithosphere Interaction during Migration of Cretaceous Alkaline Magmatism in SW Portugal: evidence from U–Pb Ages and Pb-Sr-Hf Isotopes. J. Petrol. 51, 1143–1170.
Grobe, R.W., Alvarez-Marrón, J., Glasmacher, U., Menéndez-Duarte, R., 2010. Low-temperature exhumation history of Variscan-age rocks in the western Cantabrian Mountains (NW Spain) recorded by apatite fission-track data. Tectonophysics 489, 76–90.
Hurford, A.J., Green, P.F., 1982. A users´ guide to fission track dating. Earth Planet. Sci. Lett. 59, 343–354.
Hurford, A.J., Green, P.F., 1983. The zeta age calibration of fission track dating. Chem. Geol. 1, 285–317.
Juez-Larré, J., Ter Voorde, M., 2009. Thermal impact of the break-up of Pangea on the Iberian Peninsula, assessed by thermochronological dating and numerical modeling. Tectonophysics 474, 200–213.
Julivert, M., Fontboté, M., Ribeiro, A., Conde, L.E., 1972. Mapa y memoria explicativa del Mapa Tectónico de la Península Ibérica y Baleares, scale 1:1,000,000. 113 pp., Instituto Geológico y Minero de España, Madrid.
Kali, E., Leloup, P.H., Arnaud, N., Maheo, G., Liu, D., Boutonnet, E., Van der Woerd, J., Liu, X., Liu-Zeng, J., Li, H., 2010. Exhumation history of the deepest central Himalayan rocks, Ama Drime range: key pressure-temperature-deformation time constraints on orogenic models. Tectonics 29, TC2014. http://dx.doi.org/10.1029/2009TC002551.
Keller, E.A., Pinter, N., 2002. Active Tectonics. Earthquakes, Uplift, and Landscape. Prentice Hall, New Jersey (362 pp.).
Ketcham, R.A., 2005. Forward and inverse modeling of low-temperature themochronometry data. Rev. Mineral. Geochem. 58, 275–314.
Ketcham, R.A., Donelick, R.A., Carlson, W.D., 1999. Variability of apatite fission-track annealing kinetics III: extrapolation to geological time scales. Am. Mineral. 9, 1235–1255.
Ketcham, R.A., Carter, A., Donelick, R.A., Barbarand, J., Hurford, A.J., 2007. Improved modeling of fission track annealing in apatite. Am. Min. 92, 799–810.
Kirstein, L.A., Fellin, M.G., Willett, S.D., Carter, A., Chen, Y.G., Garverz, J.I., Lee, D.C., 2010. Pliocene onset of rapid exhumation in Taiwan during arc-continent collision: new insights from detrital thermochronometry. Basin Res. 22, 270–285 10.1111/j.1365-2117.2009.00426.x.
Kohn, B.P., Gleadow, A.J.W., Brown, R.W., Gallagher, K., O'Sullivan, P.B., Foster, D.A., 2002. Shaping the Australian crust over the last 300 million years: insights from fission track thermotectonic imaging and denudation studies of key terranes. Aust. J. Earth Sci. 49, 697–717. http://dx.doi.org/10.1046/j.14400952.2002.00942.x.
Kroner, U., Romer, R.L., 2013. Two plates—many subduction zones: the Variscan orogeny reconsidered. Gondwana Res. 24, 298–329. http://dx.doi.org/10.1016/j.gr.2013.03.001.
Kullberg, J.C., 2000. Evolução Tectónica da Bacia Lusitaniana (Ph.D. Thesis) Univ. Nova de Lisboa, p. 280.
Lotze, F., 1945. Zur gliederung der Variszichen der Iberischen Meseta. Geotekt. Forsch. 6, 78–92.
Martínez-Catalán, J.R., 2011. Are the oroclines of the Variscan belt related to late Variscan strike-slip tectonics? Terra Nova 23, 241–247.
Martínez-Catalán, J.R., 2012. The Central Iberian arc, an orocline centered in the Iberian Massif and some implications for the Variscan belt. Int. J. Earth Sci. 101, 1299–1314. http://dx.doi.org/10.1007/s00531-011-0715-6.
Martínez-Catalán, J.R., Arenas, R., Díaz-García, F., Rubio-Pascual, F.J., Abati, J., Marquínez, J., 1996. Variscan exhumation of a subducted Paleozoic continental margin: the basal units of the Ordenes Complex, Galicia, NW Spain. Tectonics 15, 106–121.
Martín-González, F., Barbero, L., Capote, R., Heredia, N., Gallastegui, G., 2012. Interaction of two successive Alpine deformation fronts: constraints from low-temperature thermochronology and structural mapping (NW Iberian Peninsula). Int. J. Earth. Sci. 101, 1331–1342.
Martín-Serrano, A., 1998. El Relieve de la Región Occidental Zamorana. La Evolución Geomorfológica de un Borde del Macizo Hespérico. Instituto de Estudios Zamoranos "Florián de Ocampo" (CSIC), Diputación de Zamora, p. 306.
Marzoli, A., Renne, P.R., Piccirillo, E.M., Ernesto, M., Bellieni, G., De Min, A., Min, A., 1999. Extensive 200-million-year-old continental flood basalts of the Central Atlantic Magmatic Province. Science 284, 616–618. http://dx.doi.org/10.1126/science.284.5414.616.
Matte, P., 2001. The Variscan collage and orogeny (480–290 Ma) and the tectonic definition of the Armorica microplate: a review. Terra Nova 13, 122–128.
Miller, S.R., Sak, P.B., Kirby, E., Bierman, P.R., 2013. Neogene rejuvenation of central Appalachian topography: evidence for differential rock uplift from stream profiles and erosion rates. Earth Planet. Sci. Lett. 369-370, 1–12. http://dx.doi.org/10.1016/j.epsl.2013.04.007.
Ordóñez-Casado, B., 1998. Geochronological studies of the Pré-Mesozoic basement of the Iberian Massif: the Ossa-Morena zone and the allochtonous complexes within the Central-Iberian zone (Ph. D. thesis), Swiss Federal Institute of Technology (ETH) Zurich 12940 (235 pp.).
Ordóñez-Casado, B., Martín-Izard, A., García-Nieto, J., 2008. SHRIMP-zircon U–Pb dating of the Ni–Cu–PGE mineralized Aguablanca gabbro and Santa Olalla granodiorite: confirmation of an Early Carboniferous metallogenic epoch in the Variscan Massif of the Iberian Peninsula. Ore Geol. Rev. 34, 343–353. http://dx.doi.org/10.1016/j.oregeorev.2008.03.002.
Pereira, R., Alves, T.M., 2011. Margin segmentation prior to continental break-up: a seismic-stratigraphic record of multiphased rifting in the North Atlantic (Southwest Iberia). Tectonophysics 505, 17–34. http://dx.doi.org/10.1016/j.tecto.2011.03.011.
Pérez-Estaún, A., Bastida, F., Alonso, J.L., Marquínez, J., Aller, J., Álvarez-Marrón, J., Marcos, A., Pulgar, J.A., 1988. A thin-skinned tectonic model for an arcuate fold and thrust belt: the Cantabrian Zone (Variscan Ibero-Armorican Arc). Tectonics 7, 517–537.
Rasmussen, E.S., Lomholt, S., Andersen, C., Vejbaek, O.V., 1998. Aspects of the structural evolution of the Lusitanian Basin in Portugal and the shelf and slope area offshore Portugal. Tectonophysics 300, 199–225. http://dx.doi.org/10.1016/S0040-1951(98)00241-8.
Salvany, J.M., 2004. Tilting neotectonics of the Guadiamar drainage basin, SW Spain. Earth Surf. Process. Landf. 29, 145–160.
Schäfer, H.J., 1990. Geochronological investigations in the Ossa-Morena Zone, SW Spain Ph.D. Thesis Swiss Federal Institute of Technology (ETH), Zürichp. 153.
Schärer, U., Kornprobst, J., Beslier, M.O., Boillot, G., Girardeau, J., 1995. Gabbro and related rock emplacement beneath rifting continental-crust - U–Pb geochronological and geochemical constraints for the Galicia passive margin (Spain). Earth Planet. Sci. Lett. 130, 187–200. http://dx.doi.org/10.1016/0012-821X(94)00261-V.
Shaw, J., Johnston, S.T., Gutiérrez-Alonso, G., Weil, A.B., 2012. Oroclines of the Variscanorogen of Iberia: paleocurrent analysis and paleogeographic implications. Earth Planet. Sci. Lett. 329–330, 60–70.
Sibuet, J.C., Rouzo, S., Srivastava, S., 2012. Plate tectonic reconstructions and paleogeographic maps of the central and North Atlantic oceans. Can. J. Earth Sci. 49, 1395–1415. http://dx.doi.org/10.1139/e2012-071.
Simancas, J.F., 1983. Geología de la extremidad oriental de la Zona Surportuguesa (Ph. D. Thesis), Univ. Granada (439 pp.).
Simancas, J.F., Carbonell, R., González Lodeiro, F., Pérez Estaún, A., Juhlin, C., Ayarza, P., Kashubin, A., Azor, A., Martínez Poyatos, D., Almodóvar, G.R., Pascual, E., Sáez, R., Expósito, I., 2003. Crustal structure of the transpressional Variscan orogen of SW Iberia: SW Iberia deep seismic reflection profile (IBERSEIS. Tectonics 22, 1062. http://dx.doi.org/10.1029/2002TC001479.
Simancas, J.F., Ayarza, P., Azor, A., Carbonell, R., Martínez-Poyatos, D., Pérez-Estaún, A., González-Lodeiro, F., 2013. A seismic geotraverse across the Iberian Variscides: orogenic shortening, collisional magmatism, and orocline development. Tectonics 32, 417–432. http://dx.doi.org/10.1002/tect.20035.

Stapel, G., 1999. The nature of isostasy in western Iberia (Ph. D. Thesis), Vrije Univ, Amsterdam (148 pp.).
Tejero, R., Garzón-Heydt, G., Babín-Vich, R., Fernández-García, P., 2010. Long-term evolving "tectonic" landscapes within intra-plate domains: the Iberian Peninsula. In: Veress, B., Szigethy, J. (Eds.), Horizons in Earth Science Research vol. 2. Nova Science Publishers, pp. 103–123.
Terrinha, P., Rocha, R., Rey, J., Cachão, M., Moura, D., Roque, C., Martins, L., Valadares, V., Cabral, J., Azevedo, M.R., Barbero, L., Clavijo, E., Días, R.P., Gafeira, Matias, H., Madeira, J., Marques da Silva, C., Munhá, J., Rebelo, L., Ribeiro, C., Vicente, J., Youbi, N., 2006. A Bacia do Algarve; estratigrafía, paleogeografía e tectónica. In: Dias, R., Araújo, A., Terrinha, P., Kullberg, J.C. (Eds.), Geologia de Portugal no contexto da Ibéria. Univ. Évora, Évora (Portugal), pp. 247–316.
Tritlla, J., Solé, J., 1999. A newly-dated Cretaceous hydrothermal event in the Iberian Ranges (eastern Spain) and its significance within the Mesozoic thermal scenario in the Iberian Peninsula. Ore Geol. Rev. 15, 243–259.
Tucholke, B.E., Sawyer, D.S., Sibuet, J.C., 2007. Breakup of the Newfoundland-Iberia rift. In: Karner, G.D., Manatschal, G., Pinheiro, L.M. (Eds.), Imaging, Mapping and Modelling Continental Lithosphere Extension and Breakup vol. 282. Geological Society, London, pp. 9–46 (Special Publication).
Vázquez, M., Jabaloy, A., Barbero, L., Stuart, F.M., 2011. Deciphering tectonic- and erosion-driven exhumation of the Nevado–Filábride Complex (Betic Cordillera, Southern Spain) by low temperature thermochronology. Terra Nova 23, 257–263.
Weil, A.B., Van der Voo, R., van der Plujim, B.A., Parés, J.M., 2000. The formation of an orocline by multiphase deformation: a paleomagnetic investigation of the Cantabria-Asturias Arc (northern Spain). J. Struct. Geol. 22, 735–756.
Whittaker, A.C., 2012. How do landscapes record tectonics and climate? Lithosphere 4, 160–164. http://dx.doi.org/10.1130/RF.L003.1.
Wilson, M., 1997. Thermal evolution of the Central Atlantic passive margins: continental break-up above a Mesozoic super-plume. J. Geol. Soc. 154, 491–495.
Wolf, R.A., Farley, K.A., Kass, D.M., 1998. Modeling of the temperature sensitivity of the apatite (U–Th)/He thermochronometers. Chem. Geol. 148, 105–114. http://dx.doi.org/10.1016/S0009-2541(98)00024-2.